Effect of CNTs and Interfacial Defects on the Vibration of CNT-based Hybrid Nanotubes

Y. Xiao

Zienkiewicz Centre for Computational Engineering,
College of Engineering,
Swansea University,
Swansea Wales, SA2 8PP
599275@swansea.ac.uk

C. Y. Wang*

Zienkiewicz Centre for Computational Engineering,
College of Engineering,
Swansea University,
Swansea Wales, SA2 8PP
Chengyuan.wang@swansea.ac.uk

Y. T. Feng

Zienkiewicz Centre for Computational Engineering,
College of Engineering,
Swansea University,
Swansea Wales, SA2 8PP
Y.Feng@Swansea.ac.uk

Received 22 May 2016

Revised 12 March 2017

A hybrid nanotube (HNT) is fabricated by coating carbon nanotubes (CNTs) with a concentric coating layer. Vibration of the HNTs is of great interest due to its potential applications in nano-resonators, nanosensors/actuators and nanogenerators. In particular, it is expected that the super stiff but very light CNTs would largely up-shift the vibration frequency and improve the performance of the achieved nanodevices. On the other hand, the hybrid structures may lead to the defects at the CNT-coating layer interface, which would down-shift the frequency and impair the integrity of the HNT. This paper aims to exam these issues by using a multiple-beam model for the pristine HNTs and a finite element model for the defective ones. The frequencies are obtained for the first five modes of the HNTs reinforced by a single-wall or a multi-wall CNT. It was shown that the strengthening effect of the CNTs is substantial for the high frequency vibrations of the HNTs with a thin coating layer. In this case, the inverse effect of the interfacial defects can also be observed.

Key words: Hybrid nanotubes; carbon nanotubes; coating layer; vibration; interface defect

1. Introduction

Nanotechnology has developed rapidly in many engineering disciplines and is expected to invoke a series of technique revolutions in the 21st century. One of the most significant developments that will greatly accelerate this process is the discovery of carbon nanotubes (CNTs) [Iijima, 1991]. The superior mechanical, electronic and thermal properties of these nanotubes promise a broad range of applications in nanocomposites, nanodevices and nanoelectronics [Baughman *et al.*, 2002; Lau and Hui 2002]. In fulfilling the promises, some crucial challenges remain, such as weak attachment of CNTs to surrounding materials

* Corresponding author. Chengyuan.wang@swansea.ac.uk

[Calvert, 1999; Chen *et al.*, 2000; Seeger *et al.*, 2002; Seeger *et al.*, 2001], degradation of their superior properties in hazardous environments [Ikuno *et al.*, 2004; Kim *et al.*, 2003], agglomeration of CNTs due to the intertube van der Waals (vdW) interaction [Boccaccini *et al.*, 2006; Seeger *et al.*, 2002] and the short circuit in CNT-basednanoelectronics [Ikuno *et al.*, 2003; Wang *et al.*, 2006]. To overcome these hurdles considerable efforts [Bezryadin *et al.*, 2000; Boccaccini *et al.*, 2006; Bottini *et al.*, 2005; Calvert, 1999; Chen *et al.*, 2000; Gao *et al.*, 2003; Hu *et al.*, 2011; Hughes *et al.*, 2002; Ikuno *et al.*, 2005; Kim *et al.*, 2003; Maqbool *et al.*, 2014; Patil *et al.*, 2004; Seeger *et al.*, 2002; Seeger *et al.*, 2001; Wang *et al.*, 2006; Whitby *et al.*, 2002; Yang *et al.*, 2003; Zhang and Dai, 2000; Zhang *et al.*, 2000] have been devoted to fabricating hybrid nanotubes (HNTs) by coating CNTs with various functional materials. Recent studies confirmed that the coating materials can efficiently modify the 'inert' CNT surface, eliminate the vdW interaction between 'bare' CNTs, protect them from harmful molecules and provide insulating layer on the outer surface of CNTs [Ikuno *et al.*, 2004; Ikuno *et al.*, 2005; Kim *et al.*, 2003; Wang *et al.*, 2006].

Furthermore, the synergy of the complementary properties of CNTs and a variety of selected coating materials, e.g., transition metals [Maqbool *et al.*, 2014; Yang *et al.*, 2003; Zhang and Dai 2000; Zhang *et al.*, 2000], oxidant materials [Hu *et al.*, 2011; Ikuno *et al.*, 2004; Kim *et al.*, 2003; Seeger *et al.*, 2002; Seeger *et al.*, 2001], superconductive alloy [Yang *et al.*, 2003] and conductive polymers [Chen *et al.*, 2000; Gao, Dai and Wallace, 2003; Seeger *et al.*, 2002], provide selectable multi-functionality to HNTs. These novel HNTs thus open a vast range of entirely new and exciting applications, including spintronics that exploit the 'spin' of the electron rather than its charge, ultra-thin superconducting nanomaterials [Bezryadin *et al.*, 2000], nanosensors with diverse selectivity and extreme sensitivity [Ikuno *et al.*, 2003; Kim *et al.*, 2003; Seeger *et al.*, 2001; Wang *et al.*, 2006], (multi-tip) probes of SEM and AFM [Burt *et al.*, 2005; Hasegawa *et al.*, 2002; Ikuno *et al.*, 2004; Murata *et al.*, 2005], and other magnetic, optical and catalytic applications [Boccaccini *et al.*, 2006; Bottini *et al.*, 2005]. In view of these latest advances there exists a great expectation that the HNTs can take over CNTs as the nanofillers in composites and structural/functional elements in nanoelectronics/devices.

Similar to macroscopic structures, fulfilment of the functions of HNT-based nanostructures depend heavily on the structural integrity and the mechanics of the HNTs. As a result, understanding of their mechanical behavior is crucial for the design, fabrication and applications of HNT-based nanodevices. In 2006, Vodenitcharova and Zhang [Vodenitcharova and Zhang 2006] initiated the research by studying the bending and local buckling of the HNTs. The Airy stress-function method was employed to reveal the effect of SWCNTs' flexibility on the deformation of the HNTs. In 2011, composite beam theory was used by Wang and his co-workers [Wang and Adhikari, 2011; Wang *et al.*, 2011] to model the vibration of ZnO-CNT HNTs in the presence or absence of a radial pressure. It was demonstrated [Wang, Li and Chew, 2011] that the HNTs have the potential for pressure nanosensors. A year later, Wang's group [Zhang *et al.*, 2012] further studied the stress/strain distribution of HNTs subject to an axial load. Particular attention was given to the piezoelectric effect of the ZnO layer and the stress at the ZnO-CNT interface. In addition, an experimental study, axially compressed buckling was observed for the ZnO-CNT HNTs by Hu et.al [Hu *et al.*, 2011].

It is noted [Hu *et al.*, 2011; Wang and Adhikari, 2011; Wang *et al.*, 2011; Zhang *et al.*, 2012] that, among the fundamental issues of the HNTs are the effects of the inner CNTs and possible delamination at the coating layer-CNT interface. These issues are particularly important in the HNT vibration due to its immediate applications in nanoresonators, nanosensors/actuators and nanogenerators. The present paper thus aims to investigate and quantify the aforementioned effects on the transverse vibrations of the HNTs. The layout of the paper is as follows. In Section 2 the techniques used for the vibration analysis and calculation are developed, including a multiple-Timoshenko beam model for pristine HNTs and a finite element model for the defective HNTs. The effects of the CNTs and the interface defects are present and investigated in Section 3. New findings of the present study are summarized in Section 4.

2. Methodology of Vibration Analysis

As shown in Fig.1a the HNTs consist of an inner CNT and an outer concentric coating layer. For the specific example in Fig.1a, there exists a coating layer with thickness H and a double wall CNTs whose radius of the inner SWCNT is R_1 and that of the outer SWCNT is R_2. The coating thickness $H = R_3 - R_2$ where R_3 is the outer radius of the HNT.

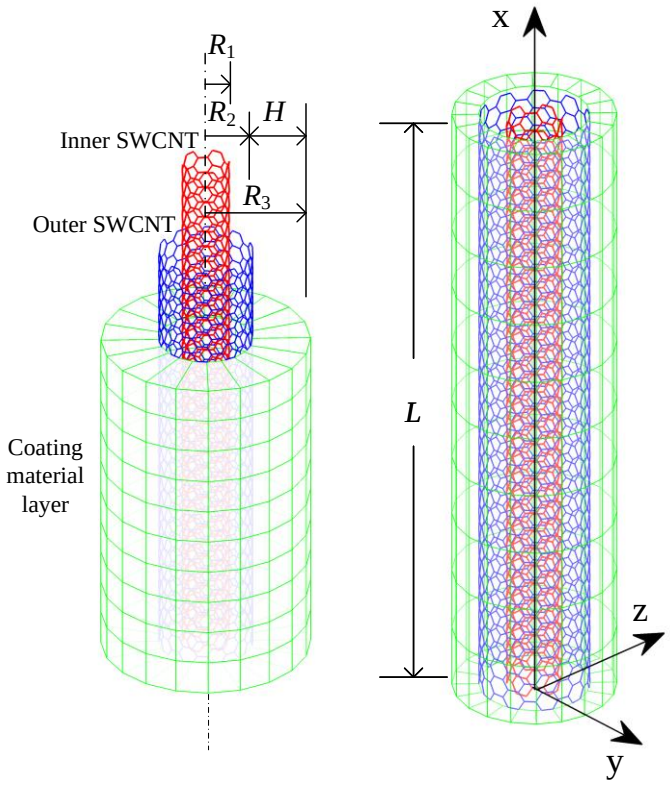

(a) (b)

Fig. 1. (a) Schematics of the structures of an HNT consisting of a double-wall CNT whose inner tube radius is R_1 and outer tube radius is R_2, and a coating layer whose thickness is H. The radius of the HNT is $R_3 = R_2 + H$. (b) Cartesian coordinate system (x, y, z) used in the study of HNTs whose length is L. Here x axis coincides with the central line of the HNT and the (y, z) plan is parallel with the cross section of the HNT.

2.1 *The multiple-beam model for pristine HNTs*

In this section the pristine HNTs (Fig.1a) are modelled based on the Timoshenko beam (TB) theory [Timoshenko, 1921; Timoshenko, 1922] which considers the effects of shear deformation and rotational inertia of the beams and thus is suitable for beams even if they have a relatively small length-to-diameter ratio. Here for a type I HNT (i.e., a coating layer + a single wall CNT (SWCNT)), the outer coating layer is considered as a hollow cylindrical TB with a thickness H and the inner SWCNT is treated as another TB with an effective thickness t_{CNT} , equivalent Young's modulus E_{CNT} and radius R_1 (the radius of the middle line). The continuity condition requires that the coating layer and the SWCNT have the same transverse displacements at their interface. Thus, a type I HNT can be modelled as a composite TB.

In the meantime, a type II HNT (i.e., a coating layer + an N-wall CNT) can be constructed by inserting N-1 SWCNTs into a type I HNT. From the innermost tube to the outmost one, the inserted N-1 SWCNTs can be labelled as TB 1, 2, …, and N-1, respectively, and the original type I HNT is considered as TB N (a composite beam). Here all SWCNTs (including the one involved in the original type I HNT) have the same effective thickness $t_{CNT}\left(=0.1nm\right)$ and equivalent Young's modulus $E_{CNT}\left(\approx 3.5TPa\right)$ [Batra and Gupta, 2008; Wang and Zhang, 2008]. The interlayer spacing or the difference in radius between the two adjacent SWCNTs is $0.34nm$. In addition, the transverse displacement w_i of TB i $(i=1,2,3,...,N-1)$ is coupled with that (those) of the adjacent TB(s) via the van der Waals (vdW) interaction p_i in the radial direction [Yoon *et al.*, 2003]. For type II HNTs the net radial pressure p_i acting on the TB i can be evaluated by

$$\begin{cases} p_1 = c_1\left(w_2 - w_1\right) \\ p_2 = c_i\left(w_{i+1} - w_i\right) - c_{i-1}(w_i - w_{i-1}) \qquad (i = 1,2,3,...,N-1) \\ p_3 = -c_{N-1}\left(w_N - w_{N-1}\right) \end{cases} \tag{1}$$

where $c_i = \dfrac{320\left(2R_i\right)}{1.6d^2}[erg/cm^2]$ $(i = 1,2,3,...,N-1)$, $d = 0.142\,nm$ and R_i is the radius of the *i*-th tube of the inner *N*-wall CNT [Wang and Adhikari, 2011]. Based on this model and the TB theory, the following vibration equations can be obtained for a type II HNT in a Cartesian coordinate system $\left(x, y, z\right)$ (Fig.1b).

$$\begin{cases} -(GA)_i k\left(\dfrac{\partial \varphi_i}{\partial x} - \dfrac{\partial^2 w_i}{\partial x^2}\right) + p_i(x) = (\rho A)_i \cdot \dfrac{\partial^2 w_i}{\partial t^2} \\ (EI)_i k \cdot \dfrac{\partial^2 \varphi_i}{\partial x^2} - (GA)_i k\left(\varphi_i - \dfrac{\partial w_i}{\partial x}\right) = (\rho I)_i \cdot \dfrac{\partial^2 \varphi_i}{\partial t^2} \end{cases} \qquad (i = 1,2,3,...,N-1) \tag{2}$$

where w_i and φ_i are the transverse deflection and the rotation angle; k (=0.8) is the shear coefficient; G is the shear modulus; E is the Young's modulus; ρ is the mass density; A denotes the area of the cross section; I represents the moment of inertia; and t is time. For TB 1, 2,… or N-1 (i.e., the inner N-1 SWCNTs) the subscript 'i' denotes the quantities of the i-th TB. For a composite TB (i.e., the N-th TB comprising the cylindrical coating layer and the outermost SWCNT), one can use Ω to denote GA , EI , ρA or ρI , and the subscripts 'coating' and 'swcnt' to represent the quantities of the coating layer and the outmost SWCNT. Then Ω can be calculated by using a general formula $\Omega = \left(\Omega\right)_{coating} + \left(\Omega\right)_{swcnt}$. The solutions to Eq. (2) can be found for such HNTs with the simply supported ends

$$w_i = A_i \sin\left(\frac{mx\pi}{L}\right) \cdot e^{i\omega t}; \quad \varphi_i = \Phi_i \cos\left(\frac{mx\pi}{L}\right) \cdot e^{i\omega t} \tag{3}$$

where A_i and Φ_i are the amplitudes of the transverse deflection and the rotation angle, respectively; ω is the angular frequency; m is the mode number (or a half wave number in the axial direction) and L is the length of the HNT (see Fig.1b). Substitution of Eq. (3) into Eq. (2) leads to the following algebraic equations

$$M\left(m,\omega\right)_{2N\times 2N}\left[A_1 \quad \Phi_1 \quad A_2 \quad \Phi_2,..., \quad A_N \quad \Phi_N\right]^T = 0 \tag{4}$$

The condition for a non-zero solution of $\left[A_1 \quad \Phi_1 \quad A_2 \quad \Phi_2,..., \quad A_N \quad \Phi_N\right]$ yields

$$\det|M\left(m,\omega\right)| = 0 \tag{5}$$

where det |.| denotes the determinant of a square matrix. By solving Eq. (5) one can obtain the frequency $f = \omega/2\pi$ as a function of mode number m. It should be pointed out that for type I HNTs, we have $i = N = 1$ in Eqs. (1) to (3), and thus only A_1 and Φ_1 are present in Eq. (4). Thus the vibration frequency of such HNTs can also be obtained by solving Eq. (5).

2.2 *Finite element model for defective HNTs*

As mentioned above, one of the objectives here is to examine the effect of the defects at the interface between the coating layer and the inner CNTs. To this end, defective HNTs with simply supported ends are considered, where, as shown in Fig.2a, a two dimensional (2D) cylindrical delamination (i.e., the thickness is zero) is introduced on the coating layer-CNT interface. The length l (= 0.9L) of the 2D defect is measured along the x direction (Fig.2a) and its cross section is an arc of the inner circular perimeter of the coating layer (Fig.2b). In the present study, the defect is assumed to be symmetric about the planes $x = \dfrac{L}{2}$ and $z = 0$. The size of the symmetric 2D defect can then be characterized by the length l and the angle θ (equally dissected by the y axis) shown in Figs.2a and b, respectively.

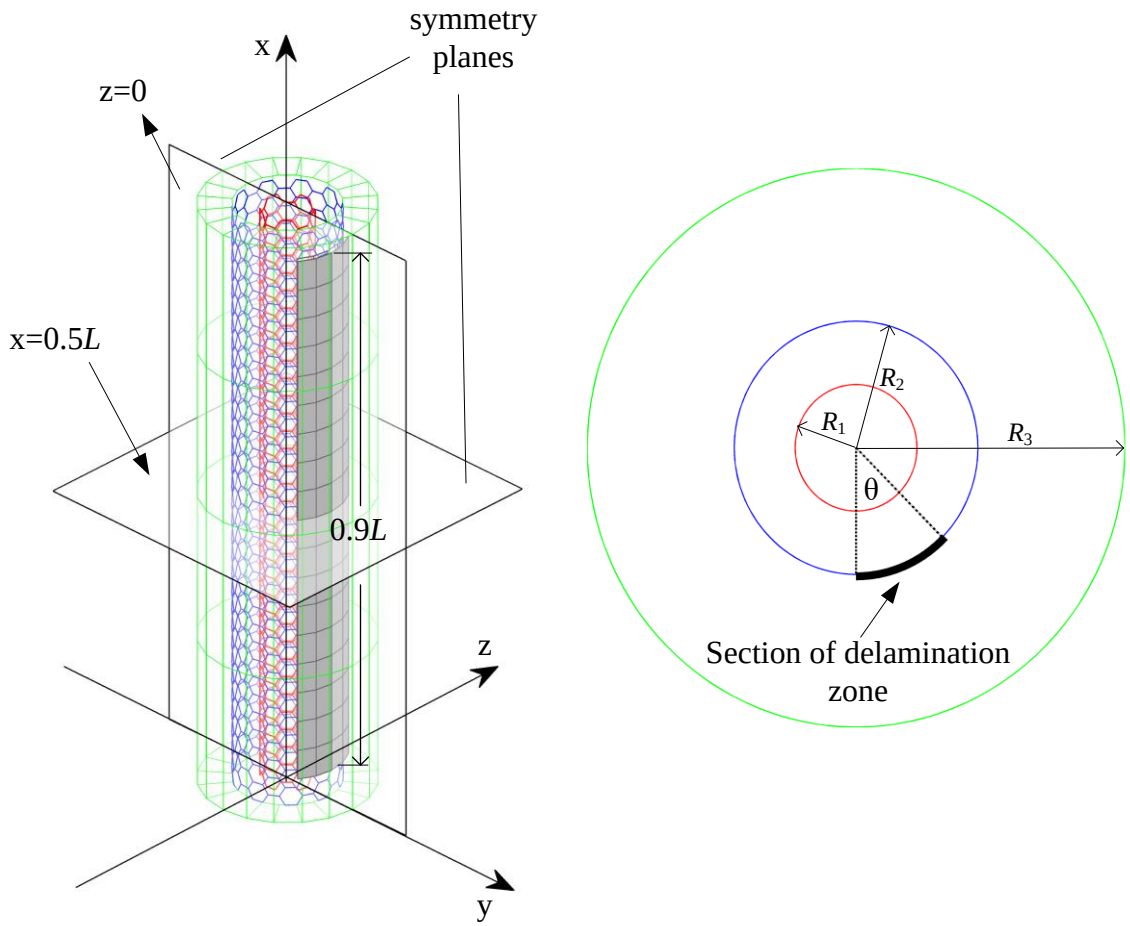

(a) (b)

Fig. 2. (a) Schematic of a defective HNT, where a 2D delamination is found on the coating layer and CNT interface. The interface defect is symmetric to the planes $x = 0.5L$ and $z = 0$. The length of the defect is $l = 0.9L$. (b) The cross section of the defective HNT and the top view of the 2D interface defect. The symmetric defect can be characterized by the length l and the angle θ .

The vibration analysis of the defective HNTs is conducted by using the finite element method (FEM) and implemented via the commercial software ANSYS. Here the cylindrical coating layer is discretized by using three dimensional elements; whereas for inner one-atom-thick SWCNTs it is performed by using 4-noded shell elements. On the coating layer-CNT interface, the 2D defect is modelled via the following two steps. First, a cylindrical cavity (the dark green area in Fig.3) is cut into the coating layer at the place where the 2D defect is introduced. The cavity has an inner lateral surface coinciding with the 2D defects at the coating layer-CNT interface, and a nonzero thickness t_{def} measured along the radial direction from its inner lateral surface to the outer one. Subsequently, the cavity is filled with an imaginary material with the same mass density as the coating material but its elastic modulus is set to zero. In this case, the mass of the coating layer remains unchanged but the stresses cannot be transferred between the coating layer and the outmost SWCNT via the defective zone. Here the smallest possible value is taken for the thickness t_{def} to minimize the possible influence of the nonzero thickness on the HNT vibration, i.e., the cavity is only one mesh element thick, more than an order of magnitude thinner than the whole coating thickness (up to $8nm$ in this study). The continuity condition is then imposed on all the interfaces between the coating layer, the defective zone and the outmost SWCNT. In ANSYS, this condition is implemented by matching the adjacent two structures at their interfaces, i.e., the two neighboring structures share the same element nodes at their interface.

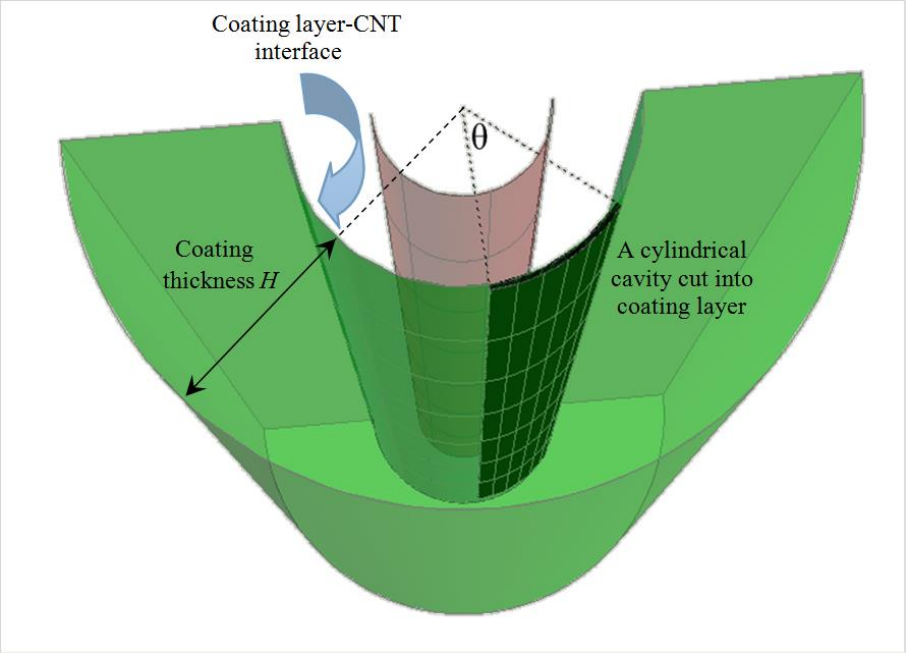

Fig. 3. Illustration of the physical model for a 2D cylindrical defect at the coating layer and CNT interface. The model is established by cutting a cylindrical cavity (the dark green zone) into the coating layer. The inner surface of the cylindrical cavity coincides with the 2D defect at the coating layer-CNT interface and the thickness is at least an order of magnitude smaller than the coating thickness *H*. The cavity is then filled with a material whose mass density is the same as the density of the coating material and its elastic moduli are zero.

In the multiple-beam model the interlayer vdW interaction of adjacent SWCNTs is considered as linear springs with an effective modulus c_i for the spring between the *i*-th and *i*+1 th SWCNTs (*i* = 1, 2, ..., *N*-1). However, the present FE model accounts for the vdW interaction by filling the space between adjacent SWCNTs with an imaginary material whose mass density, Poisson's ratio and (axial and circumferential) Young's modulus are zero. The only nonzero material property is Young's modulus $E_r (= 0.34 c_i)$ in the radial direction. In other words, the imaginary material layer is sandwiched by the two adjacent SWCNTs and able to transfer only the radial interaction between the two SWCNTs. In FEM modelling, a continuous interface is adopted between the imaginary material and adjacent SWCNTs, and implemented via the similar technique used for modelling the interface between the coating layer and outer SWCNT.

3. Results and Discussions

In this section, the techniques introduced above are employed to study the vibration of the HNTs. The objectives are to quantify the strengthening effect of the inner CNTs, and the weakening effects of the interface delamination on the structural stiffness of the HNTs. To this end, CNTs coated by Titanium (Ti) layer are considered as examples. The values of material properties used in the modelling are as follows. For SWCNTs, the equivalent Young's modulus $E_{CNT} = 3.5TPa$, the Poisson's ratio $v_{CNT} = 0.2$, and the mass density per unit lateral area $\rho_{CNT} = 2.27g/cm^3 \times 0.34nm$. For the Ti coating layer, the Young's modulus and Poisson's ratio are $E_{Ti} = 110.3GPa$ and $v_{Ti} = 0.34$, respectively. The mass density ρ_{Ti} of Ti is $4.43g/cm^3$.

3.1 *Effect of the inner CNTs*

First let us consider the effect of the CNTs on the transverse vibration of the HNTs with a perfect CNT-Ti interface. The frequencies (f_{HNT}) of the first five modes are calculated for the pristine HNTs with the coating thickness *H* varying from 0 (i.e., CNT only) to $50nm$ (Fig.1 a) and compared with the frequency (f_{Ti}) of the corresponding Ti coating layer, i.e., a hollow Ti cylinder.

3.1.1 *Type I HNTs reinforced by a thin SWCNT*

Based on the multiple-beam model f_{HNT} is first calculated as a function of the coating thickness (H) for a group of type I HNTs where the SWCNTs have a diameter $d_{CNT} = 0.68nm$ and a length-to-diameter ratio $\alpha\left(=\dfrac{L}{d_{CNT}}\right)$ equal to 40, 100 and 200, respectively. Thus, the lengths L of the HNTs (and the SWCNTs) are 27.2nm, 68nm and 136nm respectively. The frequencies f_{HNT} (solid lines) are present in Fig.4a, b and c for the HNTs of different length in comparison with the frequencies f_{Ti} of their Ti coating cylinders (dotted lines). Fig.4a shows that f_{HNT} of all the five modes (solid lines) decreases rapidly with the increase of the thickness H until it reaches a global minimum at a common critical coating thickness H_{cr} around 0.52nm. Once H exceeds the critical value H_{cr} the trend of frequency is reversed and f_{HNT} increases continuously with the increase of the thickness H. In particular, f_{HNT} associated with a larger m is found to be more sensitive to the change in the coating thickness H. On the other hand, f_{Ti} is always lower than f_{HNT}. It however increases monotonically with H and approaches f_{HNT} when H becomes sufficiently large. Obviously the strengthening effect of SWCNTs (measured by $f_{HNT} - f_{Ti}$) is substantial for the HNTs when the Ti coating layer is relatively small (e.g., $H \le H_{cr}$); it then decreases as H increases and eventually becomes small or negligible (i.e., $\beta = \dfrac{f_{HNT} - f_{Ti}}{f_{Ti}} \le 5\%$) when the Ti layer becomes relatively thick. In Fig.4, the red dotted line shows the points on the frequency curves (m = 1 to 5) at which the values of H, i.e., $H_{5\%}$, correspond to $\beta = 5\%$. In other words, the strengthening effect of the SWCNTs is negligible as long as H crosses the red dotted line to its right-hand side, i.e., $H \ge H_{5\%}$. It is also noted in Fig. 4 that H_{cr} is a constant independent of m and the length of HNTs (or the aspect ratio α of the CNT). However, $H_{5\%}$ tends to increase with the mode number m for a relatively short HNT (e.g., L = 27.2nm or $\alpha = 40$) (Fig.4a) and approaches a constant value around 1nm for relatively long HNTs (e.g., L = 68nm or $\alpha \ge 100$) (Fig.4b and c).

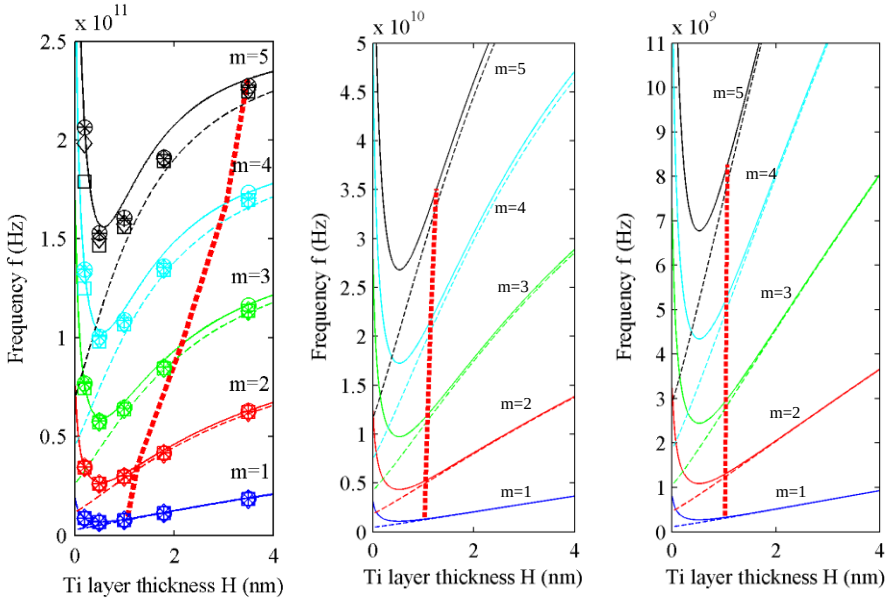

(a) (b) (c)

Fig. 4. H (the Ti thickness)-dependency of the frequencies calculated for the first five vibration modes of the type I HNTs reinforced by a thin SWCNT whose diameter $d_{CNT} = 0.68nm$ and the length-to-diameter ratio (a) $L/d_{CNT} = 40$, (b) $L/d_{CNT} = 100$ and (c) $L/d_{CNT} = 200$.

As shown above, $\beta = \frac{f_{HNT} - f_{Ti}}{f_{Ti}}$ can be utilized to quantify the strengthening effect of the inner CNTs on the vibration of the HNTs. Thus, *H*-dependence of β is plotted in Fig. 5a, b, and c for the five modes of the HNTs considered in Fig.4a, b and c, respectively. Fig. 5a shows that at $H \le H_{cr}$ β or the effect of the inner SWCNT is large but decreases swiftly with the increase of the coating thickness *H*. It however becomes smaller and much less sensitive to the variation of *H* when $H \ge H_{cr}$. For example, at $H = H_{cr}$ (0.52*nm*), β of the first five modes falls in the range of [28%, 50%]. It then reduces to [5%, 15%] when *H* approaches 1*nm*. Similar trend is observed in Fig.5b and c for the longer HNTs but β (i.e., the effect of the SWCNT) becomes much less sensitive to the mode number *m*.

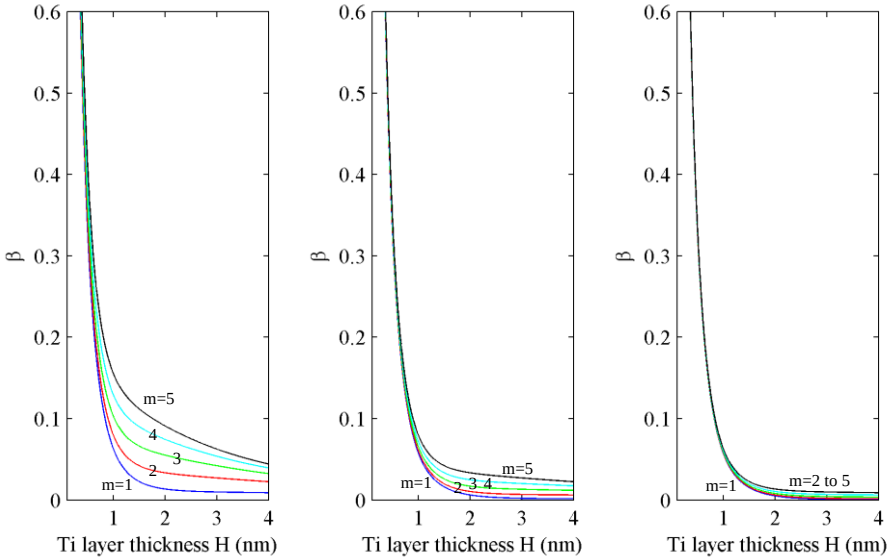

Fig. 5. The frequency ratio $\beta\left(=\frac{f_{HNT} - f_{Ti}}{f_{Ti}}\right)$ calculated against the Ti layer thickness *H* for the first five vibration modes of the type I HNTs reinforced by a thin SWCNT of $d_{CNT} = 0.68nm$, and (a) $L / d_{CNT} = 40$, (b) $L / d_{CNT} = 100$ and (c) $L / d_{CNT} = 200$.

3.1.2 *Type I HNTs reinforced by a large SWCNT*

The above results show that the thin SWCNTs with $d_{CNT} = 0.68nm$ can efficiently up-shift the frequency only when the coating layer is very thin, e.g., $H < 1nm$. One way to enhance such a strengthening effect is to increase the diameter or the structural rigidity of the SWCNTs. It is thus of interest to examine how efficient one can increase the frequency by using larger SWCNTs. In Fig. 6 f_{HNT} and the corresponding f_{Ti} are calculated for another group of type I HNTs reinforced by larger SWCNTs with $d_{CNT} = 10.04nm$ which is nearly 15 times of 0.68*nm* considered previously. In Fig.6a, b and c the aspect ratio of the SWCNT (α) also varies from 40, to 100 and 200. Accordingly, the length *L* of these HNTs is $0.4\mu m$, $1\mu m$ and $2\mu m$, respectively. It was reported that the diameter of a synthesized SWCNT is of the order of 1*nm* [Iijima and Ichihashi, 1993] and the smallest diameter ever achieved is 0.4*nm* [Qin *et al.*, 2000]. Thus SWCNTs with diameters 0.68*nm* and 10.04*nm* can be considered as the typical examples of small and large SWCNTs, respectively. In Fig. 6, the *H*-dependence of f_{HNT} and f_{Ti} is found to be qualitatively similar to those in Fig.4. Specifically, H_{cr} is again found to be independent of the length of the HNTs and the vibration mode number *m*. On the other hand, H_{cr} and $H_{5\%}$ in Fig. 6 are around 3*nm* and 6*nm* (for different *m* and α at $L \ge 1\mu m$), respectively, which is about 4 and 6 times the corresponding values (i.e., 0.52*nm* and 1*nm*) achieved in Fig.4. In the meantime, β is calculated in Fig.7 for the second group of the HNTs. Different from those in Fig.5, β -curves in Fig. 7 are insensitive to the vibration modes and the length of the HNTs. This is especially so when the length *L* increases to

$1\mu m$ or greater in Fig.7b and c, where the effect of the SWCNT changes merely with the coating thickness H. This unique feature can be attributed to the large wavelength-to-diameter ratio of the first five modes, which is 20 or even greater for the HNTs considered in Fig.7b and c.

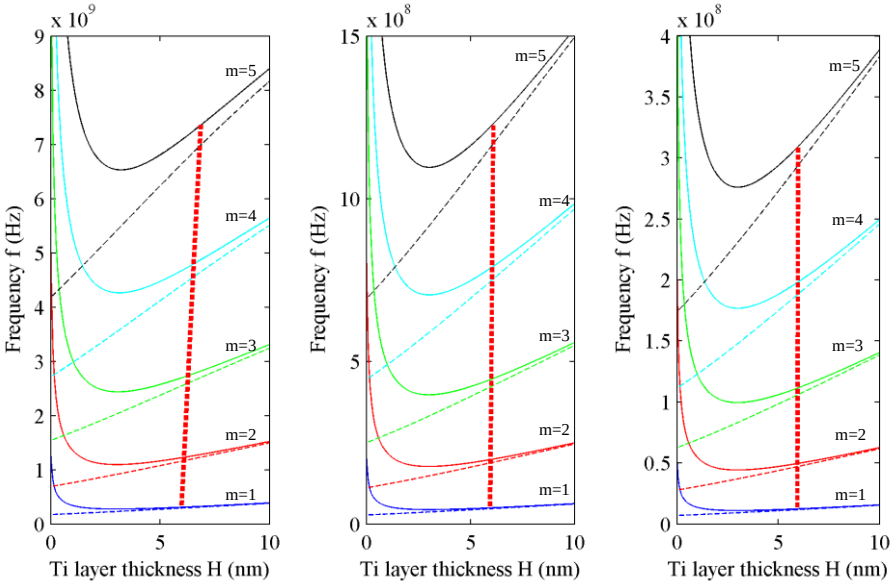

Fig. 6. H (the Ti thickness)-dependency of the frequencies calculated for the first five vibration modes of the type I HNTs reinforced by a large SWCNT whose diameter $d_{CNT} = 10.04nm$ and the length-to-diameter ratio (a) $L/d_{CNT} = 40$, (b) $L/d_{CNT} = 100$ and (c) $L/d_{CNT} = 200$.

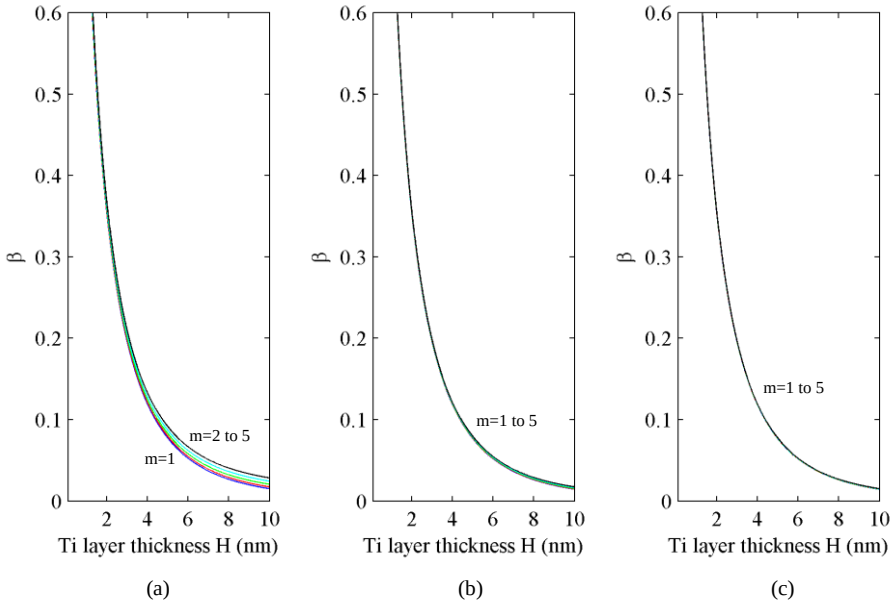

Fig. 7. The frequency ratio $\beta\left(=\frac{f_{HNT}-f_{Ti}}{f_{Ti}}\right)$ calculated against the Ti layer thickness H for the first five vibration modes of the type I HNTs reinforced by a thin SWCNT of $d_{CNT} = 10.04nm$, and (a) $L/d_{CNT} = 40$, (b) $L/d_{CNT} = 100$ and (c) $L/d_{CNT} = 200$, respectively.

3.1.3 *Type II HNTs reinforced by a MWCNT*

From Sec.3.1.2 we see that increasing d_{CNT} from 0.68*nm* to 10.04*nm* can substantially increase the upper limit of the coating thickness *H* from 0.52~1*nm* to 3~6*nm* within which the strengthening effect of the SWCNTs is strong (e.g., $\beta \geq 20\%$) or significant (e.g., $\beta \geq 5\%$). These values of *H* fall in the range of the metal-coated SWCNTs where coating thickness varies from an order of magnitude 0.5*nm* to 15*nm* [Zhang and Dai, 2000; Zhang *et al.*, 2000]. For oxide coating materials, e.g., ZnO and SiO_x, the thickness however can grow to dozens of nanometers [Ikuno *et al.*, 2005; Seeger *et al.*, 2001]. A large coating thickness (e.g., 20*nm*) may also occur for the HNTs with metallic coating. In these cases, even large SWCNTs are not stiff enough to improve the structural rigidity of the HNTs. It is thus necessary to seek an alternative way to further enhance the CNT effect on the HNTs. To this end, we have inserted up to 15 thinner SWCNTs into the second group of type I HNTs where the SWCNTs have a diameter of 10.04*nm*. f_{HNT} (also f_{Ti}) and β are calculated in Figs. 8 and 9, respectively, for the third group of the HNTs reinforced by double wall CNTs, 5-wall CNTs and 15-wall CNTs, respectively. This time, the length of the HNTs is fixed at $0.2\mu m$ and $\alpha\left(=\frac{L}{d_{CNT}}\right)$ is equal to 20.

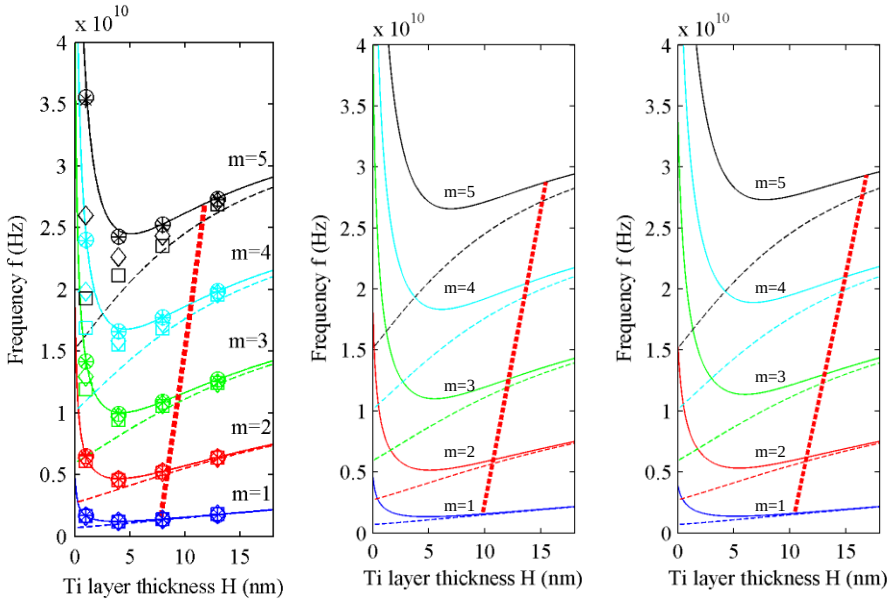

Fig. 8. *H* (the Ti thickness)-dependency of the frequencies calculated for the first five vibration modes of the type II HNTs reinforced by an *N*-wall CNT whose outmost diameter $d_{CNT}=10.04nm$ and the number of SWCNTs equals (a) *N*=2, (b) *N*=5 and (c) *N*=15.

Comparison between Figs.6 and 8 shows that H_{cr} of mode 5 increases from 3*nm* (Fig. 6) to 4.5*nm* (Fig.8a) by 50% due to the addition of a thinner SWCNT. It further increases from 4.5*nm* to 7*nm* by 55% (Fig.8b) when three more SWCNTs are inserted. However further inserting 10 more thinner SWCNTs can only increase H_{cr} from 7 to 7.8*nm* (Fig.8c) with a relative change of 14.32%. Similar trend is also observed for H_{cr} of modes 1 to 4 in Fig.8. These results indicate that the few outmost layers of an MWCNT can most efficiently enhance the strengthening effect of the inner CNTs. In addition, different from those in Fig. 6, both H_{cr} and $H_{5\%}$ in Fig. 8 increase with the modes number *m*. Consistently, Fig.9 indicates that β, i.e., the strengthening effect of the MWCNTs is sensitive to *m*. For a given *H*, β increases with the mode number *m* as well as the number of the SWCNTs inside the HNTs. It is seen from the above results that inserting up to 14 SWCNTs to form a type II HNTs reinforced by a 15-wall CNTs can substantially increases the value of H_{cr} to 7.8*nm* but it is still in the range of (0.5*nm*, 15*nm*). This is due to the fact that only a few outmost layers of the inner MWCNTs (whose diameter is limited to around 10nm) contribute significantly to the

structural stiffness. In fact, synthesized MWCNTs may have a diameter up to an order of $50nm$ or even larger, which thus would raise the structural stiffness more substantially. In other words, MWCNTs of a relatively large diameter should be employed in the design of the HNTs when a thick oxidant or metal coating layer up to dozens nanometers is considered for certain engineering applications.

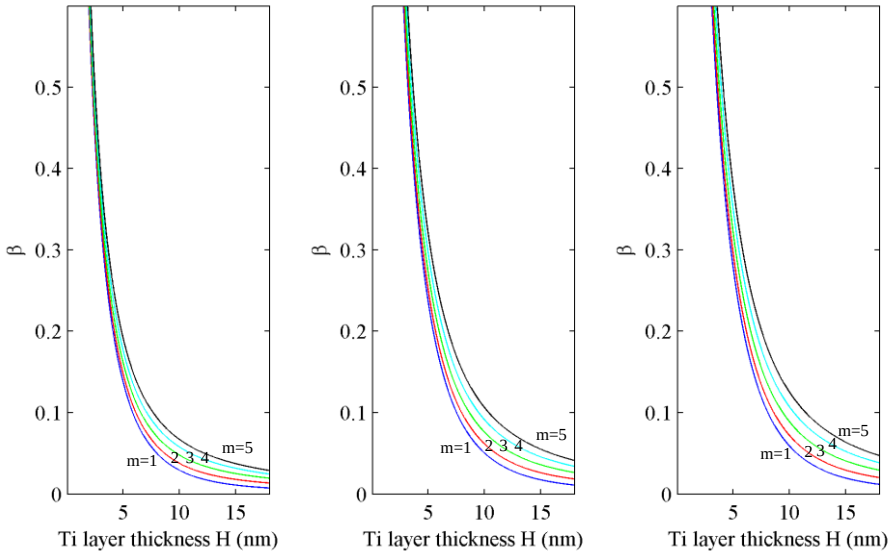

Fig. 9. The ratio The frequency ratio $\beta\left(=\frac{f_{HNT}-f_{Ti}}{f_{Ti}}\right)$ calculated against the Ti layer thickness H for the first five vibration modes of the type II HNTs reinforced by an N-wall CNT whose outmost diameter $d_{CNT}=10.04nm$ and the number of SWCNTs equals (a) N=2, (b) N=5 and (c) N=15.

3.2 *Effect of the interfacial defects*

In Section 3.1, the strengthening effect of the CNT is measured for the HNTs. Particular attention is paid to the dependency of the effect on the radius and the number of layers of the CNTs. In what follows we aim to further investigate the influence of the delamination at the interface between the Ti-coating layer and the inner CNTs.

Table 1. The relative difference between the multiple beam model and the FE model in predicting the frequency of the two examples pristine HNTs. Here example 1 is the type I HNTs reinforced by a SWCNT of diameter 0.68nm and length 27.8nm, and example 2 is the type II HNTs reinforced by a DWCNT of outer diameter 10.04nm and the length 200.8nm.

	Mode number m	The relative difference γ between two models		
		with H = 0.2nm	with H = 0.5nm	with H = 1nm
Example 1	1	1.598%	-2.287%	-3.750%
	2	1.526%	-2.311%	-4.038%
	3	1.383%	-2.425%	-4.439%
	4	1.126%	-2.614%	-4.803%
	5	0.879%	-2.673%	-5.192%
	Mode number m	The relative difference γ between two models		
		with H = 1nm	with H = 4nm	with H = 8nm
Example 2	1	0.481%	-0.250%	-0.359%
	2	-0.061%	-0.472%	-0.190%
	3	-0.841%	-0.838%	-0.001%
	4	-1.759%	-1.306%	0.056%
	5	-2.789%	-1.898%	-0.040%

To demonstrate the robustness of the FEM model developed for the HNTs (Section2.2) the vibration frequencies are calculated based on the model for the pristine HNTs (without the defect) reinforced by a SWCNT with a diameter 0.68*nm* and a length 27.8*nm* (a type I HNT), and a DWCNT with an outer diameter 10.04*nm* and a length 200.8*nm* (a type II HNT). The coating thickness H varies from 0.2*nm* up to 8*nm*. The results obtained from the FEM model and the multiple-beam model are summarized in Table 1, showing that the relative difference γ between the two models is less than 2% for relatively long type I HNTs (e.g., the length-to-diameter ratio > 17) and increases to 4~5% for relatively short ones (e.g., the length-to-diameter ratio around 10). For the type II HNTs studied γ is always smaller than 3%. This comparison shows that the present FEM model is in reasonably good agreement with the multiple-beam model for the vibrations of the pristine HNTs.

Table 2. The relative changes in frequencies δ (= $\left|\frac{f_{DH}-f_{HNT}}{f_{HNT}}\right|\times 100\%$) due to the existence of a 2D interface defect calculated for the first five modes (m = 1 to 5) of the HNTs reinforced by a SWCNT of diameter 0.68*nm* and length L = 27.2*nm*. The length l of the 2D defect is 0.9L.

Coating thickness H	Mode number m	The relative change in frequency δ (%)		
		with $\theta = 72^\circ$	with $\theta = 216^\circ$	with $\theta = 324^\circ$
0.2*nm*	1	0.057%	0.149%	0.264%
	2	0.058%	0.318%	1.098%
	3	0.052%	0.793%	3.326%
	4	0.074%	1.856%	7.424%
	5	0.097%	3.874%	13.41%
0.5*nm*	1	0.045%	0.121%	0.211%
	2	0.076%	0.305%	0.610%
	3	0.086%	0.552%	1.363%
	4	0.099%	0.994%	2.505%
	5	0.196%	1.766%	4.186%
1*nm*	1	0.039%	0.156%	0.208%
	2	0.100%	0.501%	0.701%
	3	0.232%	0.991%	1.394%
	4	0.367%	1.468%	2.202%
	5	0.436%	1.867%	2.987%
1.8*nm*	1	0.034%	0.112%	0.168%
	2	0.145%	0.580%	0.897%
	3	0.510%	0.924%	1.443%
	4	0.821%	1.657%	2.089%
	5	1.041%	1.770%	2.001%
3.5*nm*	1	0.029%	0.095%	0.122%
	2	0.047%	0.183%	0.318%
	3	0.092%	0.423%	0.590%
	4	0.381%	0.548%	0.786%
	5	0.880%	0.991%	1.001%

Subsequently, the FEM model is further employed to exam the influence of the interfacial defects on the vibration properties of the HNTs, which cannot be easily accounted for based on the multiple-beam model. Three groups of the defective HNTs are considered, where the length l of a 2D delamination is fixed at 0.9L (Fig.2a) and the angle θ is set to 72°, 216° and 324°, respectively (Fig. 2b). It is understood that the defects can only exert significant influence when the coating thickness falls in the range where the strengthening effect of CNTs is substantial, i.e., H up to around H_{cr}. Thus, for the type I HNTs reinforced by a thin SWCNT (d_{CNT} = 0.68*nm*, length L = 27.2*nm* and $H_{cr} = 0.56nm$) the frequencies are calculated for the defective HNTs with H increases from 0.2*nm* to 0.5nm and to 1*nm*. The results associated with $\theta = 72^\circ, 216^\circ$ and 324°, respectively, are represented by circles, rectangles and triangles in Fig.4a in comparison with the frequencies of the corresponding pristine HNTs (the sold lines). The relative changes in frequency

δ (= $\left|\frac{f_{DH} - f_{HNT}}{f_{HNT}}\right| \times 100\%$ where f_{DH} is the frequency of a defective HNT) associated with H = 0.2*nm*, 0.5*nm* and 1*nm* are calculated in Table 2. It is clearly seen from Fig.4a that the defects tend to reduce the structural stiffness of the HNTs and thus down-shift the frequency. In general, the frequency down-shift is found to be larger for the defective HNTs with a greater angle θ (the angle is defined in Figs. 2 and 3). This effect however is only noticeable for modes 4 and 5 but becomes insignificant for modes 1, 2 and 3. Indeed, Table 2 shows that the two greatest values of δ , i.e., 7.4% and 13.4%, are found for modes 4 and 5, respectively, at H = 0.2*nm* (the smallest H in Table 2) and $\theta = 324^\circ$ (the largest θ in Table 2). Other values in Table 2 are all smaller than 4.2%. Specifically, most of them are lower than 1%, i.e., negligibly small.

In addition to the type I HNTs, the defective type II HNTs are also investigated, where the geometric size and the constituent CNT are the same as those considered in Section 3.1.3. The interface defects considered in Fig.4a for the type I HNTs are again considered for the defective type II HNTs. In Section 3.1.3, H_{cr} obtained for the type II HNTs is around 5*nm*. Accordingly, the frequencies are calculated for the defective HNTs with the coating thickness H = 1*nm*, 4*nm* and 8*nm*, respectively. Again, the results corresponding to θ = 72°, 216°and 324° are represented in Fig.8a by circles, rectangles and triangles respectively. The relative change δ in frequency due to the defect is tabulated in Table 3 accordingly. The tendency shown in Fig. 8a is found to be similar to the one observed in Fig.4a for the type I HNTs. However, in Table 3, the effect of the defects is more pronounced than those shown in Table 2. At H = 1*nm* (the thinnest coating in Table 3) δ of mode 5 is 27% and 45% corresponding to θ =216°and 324°, respectively.

Table 3. The relative changes in frequencies δ (= $\left|\frac{f_{DH} - f_{HNT}}{f_{HNT}}\right| \times 100\%$) due to the existence of a 2D interface defect calculated for the first five modes (m = 1 to 5) of the HNTs reinforced by a double wall CNT of outer diameter 10.04*nm* and length L = 200.8*nm*. The length l of the 2D defect is 0.9L.

Coating thickness H	Mode number m	The relative change in frequency δ (%)		
		with $\theta = 72^\circ$	with $\theta = 216^\circ$	with $\theta = 324^\circ$
1*nm*	1	0.299%	0.837%	1.855%
	2	0.261%	3.065%	6.451%
	3	0.212%	8.693%	15.90%
	4	0.375%	17.51%	29.70%
	5	0.675%	26.95%	45.79%
4*nm*	1	0.166%	0.417%	0.667%
	2	0.194%	1.250%	2.069%
	3	0.242%	2.758%	5.294%
	4	0.301%	4.693%	6.558%
	5	0.329%	6.793%	13.092%
8*nm*	1	0.144%	0.360%	0.504%
	2	0.190%	0.990%	1.600%
	3	0.366%	1.832%	3.480%
	4	0.451%	2.761%	5.352%
	5	0.593%	3.678%	7.081%
13*nm*	1	0.099%	0.256%	0.317%
	2	0.183%	0.710%	1.245%
	3	0.402%	0.955%	1.568%
	4	0.440%	1.085%	2.977%
	5	0.451%	1.249%	3.362%

The values decrease to 7% and 13% at H = 4*nm*, and 3.67% and 7.08% at H = 8*nm*. In the meantime, δ at $H = 1nm$ and θ = 216°or 324° reduces to 17.5% or 29.7% as far as mode 4 is concerned. For a smaller θ or a lower frequency mode, δ in Table 3 is smaller than 1% in most cases. In other words, the influence of these defects is small and thus can normally be neglected. It should be pointed out, however, that the above results are obtained for the defects whose

length is $0.9L$, i.e., 90% of the length of the HNTs. As shown above, the effect of the delamination is small in most cases except for a few cases associated with the higher vibration mode, thin coating thickness and large angle θ.

It is easy to understand that the shorter defects would have even smaller influence on the HNTs, which is confirmed by our numerical calculations but the results are omitted here. Thus, substantial effect of the defect only occurs for the higher vibration modes of type II HNTs where the interface delamination is very large and the coating thickness is small. This is a non-intuitive result that cannot be obtained without performing the FEM simulations. Here it should be mentioned that the discrepancy between FEM (for defective HNTs) and Timoshenko beam model (for pristine HNTs) shown in Fig.4 a and 8a may partially attribute to the difference between the two modeling techniques instead of the interfacial defect. However, it is also noted that the difference shown in the two figures is much greater than the difference between the two models shown in Table 1. Thus, the comparison results in Figs.4a and 8a can adequately demonstrate the effect of the interfacial defect on the vibration of the HNTs.

4. Conclusions

A multiple beam and a finite element models are developed to characterize the vibration behavior of pristine and defective HNTs. The coating thickness-dependency is calculated for the frequency of the HNTs reinforced by a CNT, where a critical thickness H_{cr} is identified associated with the lowest frequency of the HNTs. The focus of the present study is placed on the effects of the inner CNTs and the interface defects on the vibration of HNTs. The major conclusions are summarized as follows.

Dependence of HNT frequency on the coating thickness H is calculated, where a critical value H_{cr} of coating thickness is found leading to the lowest frequency of the HNT.

The frequency up-shift due to the inner CNTs is found to be more significant for higher vibration modes of the HNTs with thinner coating thickness. Such an effect is substantial only when the coating thickness H is smaller than a critical value H_{cr} corresponding to the lowest frequency of the HNTs (i.e., the HNTs with the same inner CNT and coating material). It can be further raised by increasing the diameter and number of layers of the inner CNT. Specifically, $H_{cr} = 0.52nm$ is achieved for the HNTs reinforced by an SWCNT with $d_{CNT} = 0.68nm$. It rises to $3.0nm$ at $d_{CNT} = 10.04nm$ and further to 7.8nm when 14 thinner SWCNTs are added.

The down-shift of the HNT frequency due to the interface defects also increases with the decreasing coating thickness and increasing mode number. At $H \le H_{cr}$, the strong effect (the change in frequency up to 47%) of the defects is achieved for the modes 4 and 5 of the defective HNTs with the angle $\theta \ge 216^{\circ}$ and the length $l \ge 0.9L$. The effect however turns out to be very small or negligible (e.g., the change in frequency smaller than 1%) for lower vibration modes of the defective HNTs with smaller defects or thicker coating thickness.

It is noted that the outcomes of this work may significantly broaden the knowledge of the mechanical behavior of the HNTs and provide cost-effective modeling techniques for vibration analysis of HNTs, which have the potential to be further extended to the buckling and static deformation of the HNTs. These results thus are expected to provide useful guidance for the study, design and fabrication of the HNTs in the near future.

References

Batra, R. and Gupta, S. [2008] "Wall thickness and radial breathing modes of single-walled carbon nanotubes," *Journal of applied mechanics* **75**(6), 061010.

Baughman, R.H., Zakhidov, A.A. and De Heer, W.A. [2002] "Carbon nanotubes--the route toward applications," *Science* **297**(5582), 787-792.

Bezryadin, A., Lau, C. and Tinkham, M. [2000] "Quantum suppression of superconductivity in ultrathin nanowires," *Nature* **404**(6871), 971-974.

Boccaccini, A.R., Cho, J., Roether, J.A., Thomas, B.J., Minay, E.J. and Shaffer, M.S. [2006] "Electrophoretic deposition of carbon nanotubes," *Carbon* **44**(15), 3149-3160.

Bottini, M., Tautz, L., Huynh, H., Monosov, E., Bottini, N., Dawson, M.I., Bellucci, S. and Mustelin, T. [2005] "Covalent decoration of multi-walled carbon nanotubes with silica nanoparticles," *Chem. Commun* **43**(6)., 758-760.

Burt, D.P., Wilson, N.R., Weaver, J.M., Dobson, P.S. and Macpherson, J.V. [2005] "Nanowire probes for high resolution combined scanning electrochemical Microscopy-Atomic force Microscopy," *Nano Letters* **5**(4), 639-643.

Calvert, P. [1999] "Nanotube composites: a recipe for strength," *Nature* **399**(6733), 210-211.

Chen, G.Z., Shaffer, M.S., Coleby, D., Dixon, G., Zhou, W., Fray, D.J. and Windle, A.H. [2000] "Carbon nanotube and polypyrrole composites: coating and doping," *Advanced Materials* 12(7), 522-526.

Gao, M., Dai, L. and Wallace, G.G. [2003] "Biosensors based on aligned carbon nanotubes coated with inherently conducting polymers," *Electroanalysis* **15**(13), 1089-1094.

Hasegawa, S., Shiraki, I., Tanabe, F. and Hobara, R. [2002] "Transport at surface nanostructures measured by four-tip STM," *Current Applied Physics* **2**(6), 465-471.

Hu, C.J., Lin, Y.H., Tang, C.W., Tsai, M.Y., Hsu, W.K. and Kuo, H.F. [2011] "ZnO- Coated Carbon Nanotubes: Flexible Piezoelectric Generators," *Advanced Materials* **23**(26), 2941-2945.

Hughes, M., Shaffer, M.S., Renouf, A.C., Singh, C., Chen, G.Z., Fray, D.J. and Windle, A.H. [2002] "Electrochemical capacitance of nanocomposite films formed by coating aligned arrays of carbon nanotubes with polypyrrole," *Advanced Materials* **14**(5), 382-385.

Iijima, S. [1991] "Helical microtubules of graphitic carbon," *Nature* **354**(6348), 56-58.

Iijima, S. and Ichihashi, T. [1993] "Single-shell carbon nanotubes of 1-nm diameter," *Nature* **364**(6439), 737-740.

Ikuno, T., Katayama, M., Kamada, K., Honda, S.I., Lee, J.G., Mori, H. and Oura, K. [2003] "Insulator-coated carbon nanotubes synthesized by pulsed laser deposition," *Japanese journal of applied physics* **42**(11B), L1356.

Ikuno, T., Katayama, M., Kishida, M., Kamada, K., Murata, Y., Yasuda, T., Honda, S.I., Lee, J.G., MORI, H. AND OURA, K. [2004] "Metal-coated carbon nanotube tip for scanning tunneling microscope," *Japanese journal of applied physics* **43**(5A), L644.

Ikuno, T., Yasuda, T., Honda, S.I., Oura, K., Katayama, M., Lee, J.G. and Mori, H. [2005] "Coating carbon nanotubes with inorganic materials by pulsed laser deposition," *Journal of applied physics* **98**(11), 114305.

Kim, W., Javey, A., Vermesh, O., Wang, Q., Li, Y. and Dai, H. [2003] "Hysteresis caused by water molecules in carbon nanotube field-effect transistors," *Nano Letters* **3**(2), 193-198.

Lau, A.K.T. and Hui, D. [2002] "The revolutionary creation of new advanced materials—carbon nanotube composites," *Composites Part B: Engineering* **33**(4), 263-277.

Maqbool, A., Khalid, F.A., Hussain, M.A. and Bakhsh, N. [2014] "Synthesis of copper coated carbon nanotubes for aluminium matrix composites," *In IOP Conference Series: Materials Science and Engineering IOP Publishing*, 012040.

Murata, Y., Yoshimoto, S., Kishida, M., Maeda, D., Yasuda, T., Ikuno, T., Honda, S.I., Okado, H., Hobara, R. and Matsuda, I. [2005] "Exploiting metal coating of carbon nanotubes for scanning tunneling microscopy probes," *Japanese journal of applied physics* **44**(7S), 5336.

Patil, A., Sippel, J., Martin, G.W. and Rinzler, A.G. [2004] "Enhanced functionality of nanotube atomic force microscopy tips by polymer coating," *Nano Letters* **4**(2), 303-308.

Qin, L.C., Zhao, X., Hirahara, K., Miyamoto, Y., Ando, Y. and Iijima, S. [2000] "Materials science: The smallest carbon nanotube," *Nature* **408**(6808), 50-50.

Seeger, T., K Hler, T., Frauenheim, T., Grobert, N., Rhle, M., Terrones, M. and Seifert, G. [2002] "Nanotube composites: novel SiO 2 coated carbon nanotubes," *Chemical Communications* **76**(1), 34-35.

Seeger, T., Redlich, P., Grobert, N., Terrones, M., Walton, D., Kroto, H.W. and Rhle, M. [2001] "SiO x-coating of carbon nanotubes at room temperature," *Chemical Physics Letters* **339**(1), 41-46.

Timoshenko, S.P. [1921] "LXVI. On the correction for shear of the differential equation for transverse vibrations of prismatic bars," *The London, Edinburgh, and Dublin Philosophical Magazine and Journal of Science* **41**(245), 744-746.

Timoshenko, S.P. [1922] "X. On the transverse vibrations of bars of uniform cross-section," *The London, Edinburgh, and Dublin Philosophical Magazine and Journal of Science* **43**(253), 125-131.

Vodenitcharova, T. and Zhang, L. [2006] "Bending and local buckling of a nanocomposite beam reinforced by a single-walled carbon nanotube," *International Journal of Solids and Structures* **43**(10), 3006-3024.

Wang, C.Y. and Adhikari, S. [2011] "ZnO-CNT composite nanotubes as nanoresonators," *Physics Letters A* **375**(22), 2171-2175.

Wang, C., Li, L. and Chew, Z. [2011] "Vibrating ZnO–CNT nanotubes as pressure/stress sensors," *Physica E: Low-dimensional Systems and Nanostructures* **43**(6), 1288-1293.

Wang, C. and Zhang, L. [2008] "An elastic shell model for characterizing single-walled carbon nanotubes," *Nanotechnology* **19**(19), 195704.

Wang, J., Khlobystov, A.N., Wang, W., Howdle, S.M. and Poliakoff, M. [2006] "Coating carbon nanotubes with polymer in supercritical carbon dioxide," *Chemical Communications* **18**(15), 1670-1672.

Whitby, R., Hsu, W., Boothroyd, C., Kroto, H. and Walton, D. [2002] "Tungsten disulphide coated multi-walled carbon nanotubes," *Chemical Physics Letters* **359**(1), 121-126.

Yang, C.K., Zhao, J. and Lu, J.P. [2003] "Magnetism of transition-metal/carbon-nanotube hybrid structures," *Physical Review Letters* **90**(25), 257203.

Yoon, J., Ru, C. and Mioduchowski, A. [2003] "Vibration of an embedded multiwall carbon nanotube," *Composites Science and Technology* **63**(11), 1533-1542.

Zhang, J., Wang, R. and Wang, C. [2012] "Piezoelectric ZnO-CNT nanotubes under axial strain and electrical voltage," *Physica E: Low-dimensional Systems and Nanostructures* **46**, 105-112.

Zhang, Y. and Dai, H. [2000] "Formation of metal nanowires on suspended single-walled carbon nanotubes," *Applied Physics Letters* **77**(19), 3015-3017.

Zhang, Y., Franklin, N.W., Chen, R.J. and Dai, H. [2000] "Metal coating on suspended carbon nanotubes and its implication to metal–tube interaction," *Chemical Physics Letters* **331**(1), 35-41.